


## Collective Quantum Memory Activated by a Driven Central Spin

Emil V. Denning<sup>1,2</sup>, Dorian A. Gangloff,<sup>2</sup> Mete Atatüre,<sup>2</sup> Jesper Mørk,<sup>1</sup> and Claire Le Gall<sup>2,\*</sup><sup>1</sup>Department of Photonics Engineering, Technical University of Denmark, 2800 Kongens Lyngby, Denmark<sup>2</sup>Cavendish Laboratory, University of Cambridge, JJ Thomson Avenue, Cambridge CB3 0HE, United Kingdom (Received 11 April 2019; published 2 October 2019)

Coupling a qubit coherently to an ensemble is the basis for collective quantum memories. A single driven electron in a quantum dot can deterministically excite low-energy collective modes of a nuclear spin ensemble in the presence of lattice strain. We propose to gate a quantum state transfer between this central electron and these low-energy excitations—spin waves—in the presence of a strong magnetic field, where the nuclear coherence time is long. We develop a microscopic theory capable of calculating the exact time evolution of the strained electron-nuclear system. With this, we evaluate the operation of quantum state storage and show that fidelities up to 90% can be reached with a modest nuclear polarization of only 50%. These findings demonstrate that strain-enabled nuclear spin waves are a highly suitable candidate for quantum memory.

DOI: 10.1103/PhysRevLett.123.140502

**Introduction.**—Quantum memory working in conjunction with a computational qubit is a central element in fault-tolerant quantum computing and communication strategies [1,2]. Prominent examples of quantum memory implementations include collective states of atomic ensembles [3–6] and rare-earth-ion doped crystals [7,8] able to store a photonic qubit, cold ions, where the decoherence-free subspace of a local ion pair acts as memory for a single ion qubit [9,10] and nitrogen vacancy centers in diamond, where the electronic spin state can be written into a single proximal nuclear spin [11–13]. For semiconductor quantum dots, the mesoscopic spin environment comprising  $\sim 10^4$ – $10^5$  nuclei is a candidate for a collective quantum memory that can store the electronic spin state [14–16], with the promise of coherence times reaching milliseconds [17]. A strategy for electron-nuclear state transfer is based on flip flops generated by the collinear hyperfine interaction [14]. A consequence of this interaction scheme brings about opposing requirements: Vanishing electron spin splitting during the state transfer vs large electron spin splitting to polarize and stabilize the nuclear coherence [18]. An alternative approach is to use collective nuclear spin wave excitations that have recently been observed under a strong magnetic field in the form of a coherently distributed single nuclear spin excitation [19] through an effective noncollinear hyperfine interaction [20]. In this Letter, we propose a protocol for quantum memory based on this interaction, which in equilibrium is suppressed by a strong static magnetic field, but can be controllably switched on for a finite time by driving the qubit out of equilibrium.

The noncollinear hyperfine interaction responsible for qubit-controlled spin wave excitation originates from strain. In a strained lattice [cf. Fig. 1(a)], the induced electric field gradient couples to the quadrupole moment of

the nuclei, thereby tilting the nuclear spin quantization axis away from that dictated by the magnetic field (defining the  $z$  axis). This strain-induced mixing of the Zeeman eigenstates allows otherwise forbidden nuclear transitions that

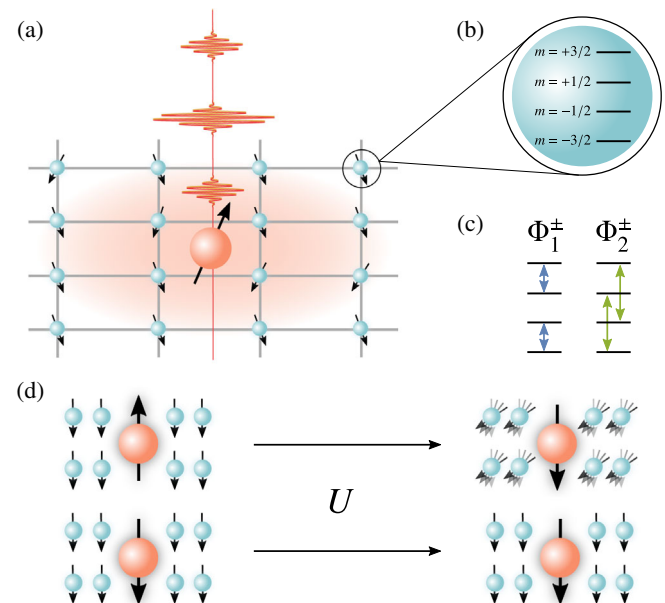


FIG. 1. (a) System schematic comprising a pulse-driven electron coupled to a mesoscopic bath of nuclear spins. (b) Structure of the high-spin ( $I > 1/2$ ) nuclei, here shown for  $I = 3/2$ . (c) Spin transitions between states in (b) generated by the noncollinear processes  $\Phi_1^\pm$  and  $\Phi_2^\pm$ . (d) In the memory write-in process, the stimulated electron-nuclear interaction flips the electron and generates a nuclear spin wave conditionally on the electron spin, thereby transferring the electron state to the nuclear ensemble. Here, the time-evolution operator,  $U = e^{-i\mathcal{H}_t\pi/(2g_c)}$ , corresponds to the evolution in Eq. (2) at time  $t = \pi/(2g_c)$ .

can be accessed by the electron through the hyperfine interaction,  $H_{\text{hf}} = \sum_j 2A^j I_z^j S_z$  ( $S_z$  and  $I_z^j$  are electronic and  $j$ th nuclear spin- $z$  operators). The transitions are activated when the electron spin is driven—magnetically or optically—to bridge the excitation energy gap corresponding to the nuclear Zeeman energy,  $\omega_Z^n$ .

Equipped with an interaction mechanism that can be switched on and off, information can be controllably transferred from the electron to the nuclei by letting the two subsystems interact for a finite duration. This can be realized in multiple ways; for the current proposal, we consider a Hamiltonian engineering approach based electron spin rotations on the Bloch sphere with a sequence of fast pulses [21], which selectively enhances the collective electron-nuclear transitions and simultaneously cancels out slow noise from the nuclear Overhauser field. The electron spin rotations in the pulse sequence can be carried out using an all-optical Raman drive to obtain phase-controlled manipulation at Rabi frequencies far exceeding the nuclear Zeeman splitting and hyperfine fluctuations of the electron Zeeman energy [22]. The nuclear coherence time can be extended up to milliseconds by removing the electron from the quantum dot [18] or alternatively by decoupling of the Knight field through a simple electron spin echo sequence [23,24]. Readout of the nuclear memory is effectuated by once again driving the electron to turn on the interaction.

*Electron-nuclear exchange mechanism.*—The Hamiltonian describing the quadrupolar coupling of the  $N$  nuclear spins ( $I > 1/2$ ) is

$$H_Q = \sum_{j=1}^N B_Q [(I_x^j)^2 \sin^2 \theta + \frac{1}{2} (I_x^j I_z^j + I_z^j I_x^j) \sin 2\theta + (I_z^j)^2 \cos^2 \theta],$$

where  $I_\alpha^j$ ,  $\alpha = x, y, z$  are the spin operators of the  $j$ th nucleus,  $\theta$  is the tilt angle of the quadrupolar axis away from  $z$ , and  $B_Q$  is the quadrupolar interaction strength. The low-energy excitations of the system are obtained through a Schrieffer-Wolff transformation perturbative in  $B_Q/\omega_Z^n$ , which replaces  $H_Q$  by  $H_Q^0 + V_Q'$ .  $H_Q^0$  commutes with  $I_z^j$  and  $V_Q' = S_z [\mathcal{A}_1 (\Phi_1^+ + \Phi_1^-) + \mathcal{A}_2 (\Phi_2^+ + \Phi_2^-)]$  is a noncollinear hyperfine interaction [19,25]. Here,  $\Phi_\zeta^\pm$  ( $\zeta = 1, 2$ ) denotes the nuclear spin wave operators

$$\Phi_1^+ = \sum_j a_j [I_+^j I_z^j + I_z^j I_+^j], \quad \Phi_2^+ = \sum_j a_j (I_+^j)^2,$$

with  $\Phi_\zeta^- = (\Phi_\zeta^+)^\dagger$ ; thus  $\Phi_\zeta^\pm$  changes the net nuclear spin by  $\pm \zeta$  as shown in Figs. 1(b)–1(c). The overall strength of the interaction is given by  $\mathcal{A}_1 = \frac{1}{2} \sum_j A^j B_Q \sin 2\theta / \omega_Z^n$  and  $\mathcal{A}_2 = \frac{1}{2} \sum_j A^j B_Q \sin^2 \theta / \omega_Z^n$ , and  $a_j = A^j / \sum_j A^j$  are the normalized hyperfine coefficients. A quadrupolar coupling

strength of  $B_Q = 1.5$  MHz, which is typical of naturally occurring strain [30] or which can be engineered *in situ* [31,32], will be considered here.

A nuclear spin transition corresponding to the action of  $\Phi_\zeta^\pm$  costs an energy of  $\zeta \omega_Z^n$ , which in a strong magnetic field is considerably larger than the transition matrix elements of  $V_Q'$ . Consequently, these processes are far off resonance in equilibrium. To switch the interaction on, we follow Ref. [21] and consider the action of a pulse sequence on the electron spin, driving it with a set of short  $S_x$  and  $S_y$  pulses separated by a time interval,  $\tau/4$ . By setting  $\tau = \ell \pi / (\zeta \omega_Z^n)$ , where  $\ell$  is an odd integer, the coupling between the electron and the  $\Phi_\zeta$  mode is resonantly enhanced, and the system will evolve under an effective flip-flop Hamiltonian [25]

$$\mathcal{H}_I = \mathcal{A}'_\zeta (\Phi_\zeta^+ S_- + \Phi_\zeta^- S_+), \quad (1)$$

where  $S_\pm = S_x \pm i S_y$  are the electron spin-flip operators and  $\mathcal{A}'_\zeta$  is a rescaled coupling rate taking its maximal value for  $\ell = 3$ , where  $\mathcal{A}'_\zeta = (2 + \sqrt{2}) / (3\pi) \mathcal{A}_\zeta$ . When the nuclei are initialized in a fully polarized state, this Hamiltonian will create a nuclear spin wave and flip the electron spin conditionally on the electron spin state [see Fig. 1(d)], thus forming the basis of information transfer between the electron and nuclear ensemble. While realistic quantum dots comprise nuclei of several species, we show [25] that under a magnetic field sufficiently strong to energetically resolve each species, the pulse sequence can couple the electron to a single species.

To see how this protocol turns nuclear spins into a quantum memory, we first consider a perfectly polarized nuclear bath [see Fig. 2(a)]. We write this nuclear state as  $|\mathbf{0}\rangle = |-I, \dots, -I\rangle$ , and take the electron to be initialized in the state  $|\phi\rangle = \alpha |\uparrow\rangle + \beta |\downarrow\rangle$ , which we want to transfer to the nuclei. Because the nuclei are initialized in the ground state, no downwards transitions are possible and  $\Phi_\zeta^- |\mathbf{0}\rangle = 0$ . The excited nuclear state  $|\mathbf{1}\rangle \propto \Phi_\zeta^+ |\mathbf{0}\rangle$  is a distributed superposition of nuclear excitations [indicated by blue dots in Fig. 2(a)],  $\sum_j a_j |-I, \dots, (-I + \zeta)_j, \dots, -I\rangle$ . Crucially, when deexciting the spin wave, the only downwards nuclear transitions available are those that were excited from the ground state, and thus  $\Phi_\zeta^- |\mathbf{1}\rangle \propto |\mathbf{0}\rangle$ . Because of these properties, the system evolves within a three dimensional subspace as

$$|\psi(t)\rangle = \alpha [\cos(g_\zeta t) |\uparrow\rangle \otimes |\mathbf{0}\rangle - i \sin(g_\zeta t) |\downarrow\rangle \otimes |\mathbf{1}\rangle] + \beta |\downarrow\rangle \otimes |\mathbf{0}\rangle, \quad (2)$$

$g_\zeta = F_\zeta \mathcal{A}'_\zeta \sqrt{\sum_j a_j^2}$  (scaling as  $\sqrt{N}$ ) is a collectively enhanced noncollinear coupling rate, where  $F_1 = (1 - 2I)\sqrt{2I}$ ,  $F_2 = 2\sqrt{I(2I - 1)}$ . At time  $t = \pi / (2g_\zeta)$

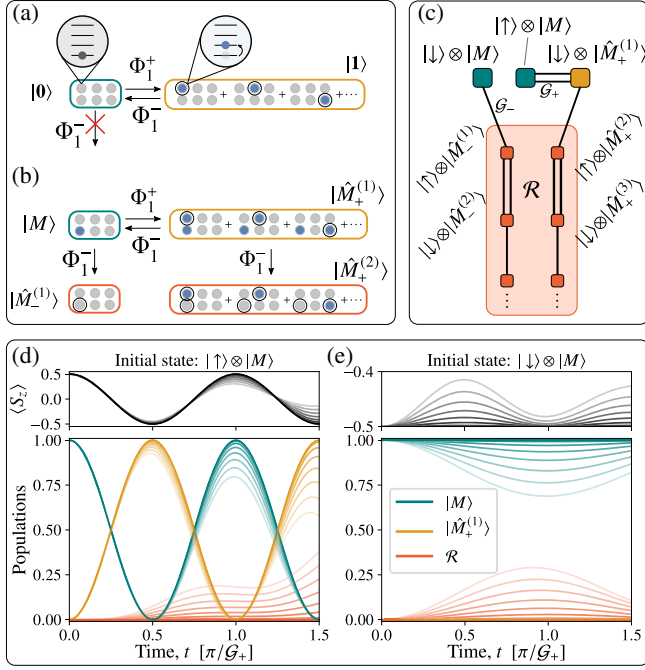


FIG. 2. (a) Collective spin wave excitation starting from a fully polarized state, where all nuclei are in the ground state (gray dots). The black circles emphasize the nuclei that have exchanged energy with the electron. The spin wave contains a single nuclear excitation (blue dots) distributed among all of the nuclei in a superposition. (b) Spin wave excitation from finitely polarized nuclear product state  $|M\rangle$  to target state  $|\hat{M}_+^{(1)}\rangle$ , where initially excited nuclei allow leakage transitions, respectively, to orthogonal states  $|\hat{M}_-^{(1)}\rangle$  and  $|\hat{M}_+^{(2)}\rangle$ . (c) Coupling structure in 1D mapping of nuclear state space. The initial state is a superposition of the two green states, and interactions couple these initial states to a 1D structure of states. Double lines signify the fast coupling rate  $\mathcal{G}_+$ , and single lines the slow rate,  $\mathcal{G}_-$ . For a fully polarized ensemble  $\mathcal{G}_- = 0$  and the three upper states remain isolated; at finite polarization, this subspace is coupled to the residual chain of states,  $\mathcal{R}$ . (d)–(e) Dynamics for initialization in electron states  $|\uparrow\rangle$  and  $|\downarrow\rangle$ , respectively. Solid lines signify the fully polarized case, where  $\mathcal{G}_- = 0$ . Lines with decreased opacity signify decreased polarization and thus an increased  $\mathcal{G}_-$  rate, with the maximal value  $\mathcal{G}_-/\mathcal{G}_+ = 0.3$ . Line colors correspond to states in panel (c).

the electron-nuclear wave function separates,  $|\psi(\pi/2g_\zeta)\rangle = |\downarrow\rangle \otimes (-i\alpha|\mathbf{0}\rangle + \beta|\mathbf{1}\rangle)$ , and the electron state is identically transferred to the collective state of the nuclei to be stored.

*Operation at partial nuclear polarization.*—A realistic implementation will initialize the nuclei in a partially polarized state [33],  $|M\rangle = |m_1, \dots, m_N\rangle$ , such that there is a small number of lower energy states to scatter into, and thus  $\Phi_\zeta^-|M\rangle \neq 0$  [see Fig. 2(b)]. Accordingly, the downwards transition  $|M\rangle \rightarrow \Phi_\zeta^-|M\rangle$  is no longer forbidden as in the perfectly polarized case, but will take place with a rate  $\mathcal{G}_-$ , which is slower than the upwards coupling rate  $\mathcal{G}_+$ . Similarly, the downwards transition  $\Phi_\zeta^-$  from the excited state  $\Phi_\zeta^+|M\rangle$  does not lead back to  $|M\rangle$  but mixes with other

states generated by deexcitation of the initially unpolarized nuclei. This leads to dephasing of the spin wave mode serving as quantum memory. Nonetheless, the asymmetry of the coupling rates ( $\mathcal{G}_+ > \mathcal{G}_-$ ) makes it possible to operate the quantum memory at finite polarizations.

To calculate the electron-nuclear dynamics during the pulse sequence, we have developed a numerically exact technique that maps the nuclear many-body state onto two one-dimensional chains of states,  $\hat{\mathcal{S}}_\pm = \{|\hat{M}_\pm^{(k)}\rangle | k=0, \dots, N\}$ . Here, the initial state  $|\hat{M}_+^{(0)}\rangle = |\hat{M}_-^{(0)}\rangle = |M\rangle$  appears as the first link in both chains. The set  $\hat{\mathcal{S}}_+$  ( $\hat{\mathcal{S}}_-$ ) represents the set of states tied with the evolution of a positive (negative) spin wave. The coupling structure of  $\mathcal{H}_I$ , taking the electron spin into account as well, is illustrated in Fig. 2(c), where a coupling rate of  $\mathcal{G}_+$  between two neighboring states is depicted with a double line and  $\mathcal{G}_-$  with a single line. In the Supplemental Material [25] we derive the form of the basis sets  $\hat{\mathcal{S}}_\pm$  and show that only neighboring nuclear states are coupled by the spin wave operators entering  $\mathcal{H}_I$ ,

$$\begin{aligned} \langle \hat{M}_+^{(2n\pm 1)} | \Phi_\zeta^+ | \hat{M}_+^{(2n)} \rangle &= \langle \hat{M}_-^{(2n)} | \Phi_\zeta^+ | \hat{M}_-^{(2n\mp 1)} \rangle = \mathcal{G}_\pm / \mathcal{A}_\zeta^+, \\ \langle \hat{M}_+^{(2n)} | \Phi_\zeta^- | \hat{M}_+^{(2n\pm 1)} \rangle &= \langle \hat{M}_-^{(2n\mp 1)} | \Phi_\zeta^- | \hat{M}_-^{(2n)} \rangle = \mathcal{G}_\pm / \mathcal{A}_\zeta^-. \end{aligned} \quad (3)$$

The asymmetry in rates is parametrized by a leakage factor  $\mathcal{G}_-/\mathcal{G}_+$ , which indicates the extent to which the nuclear phase space is explored in the evolution. In the fully polarized case, where the initial state is  $|M\rangle = |\mathbf{0}\rangle$  (and  $|\hat{M}_+^{(1)}\rangle = |\mathbf{1}\rangle$ ), we find  $\mathcal{G}_+ = g_\zeta$ ,  $\mathcal{G}_- = 0$  (no leakage), meaning that the three states  $|\uparrow\rangle \otimes |M\rangle$ ,  $|\downarrow\rangle \otimes |\hat{M}_+^{(1)}\rangle$ ,  $|\downarrow\rangle \otimes |M\rangle$  are completely decoupled from the residual part of the two chains [which in Fig. 2(c) is signified by  $\mathcal{R}$ ], recovering the ideal state transfer dynamics of Eq. (2). For finite initial nuclear polarization, we generally have  $\mathcal{G}_+ < g_\zeta$  and  $\mathcal{G}_- > 0$  (finite leakage), and thus the three states couple to the residual chains,  $\mathcal{R}$ . Figures 2(d)–2(e) show the electron and nuclear dynamics as the leakage factor  $\mathcal{G}_-/\mathcal{G}_+$  is gradually changed from the ideal case of 0 (solid lines) to 30% in linear steps (decreasing opacity). As  $\mathcal{G}_-$  is increased, the system is more rapidly delocalized along the chain, leading to uncontrollable electron-nuclear correlations that are seen as damped oscillations in the nuclear and electronic populations. When calculating the dynamics, it is necessary to truncate the nuclear chains of states to a certain  $k$  index,  $k^*$ . As long as the occupation of the states  $|\hat{M}_\pm^{(k^*)}\rangle$  is sufficiently small, the truncation remains a valid approximation. The necessary value of  $k^*$  needed for convergence depends on the evolution time and the leakage factor  $\mathcal{G}_-/\mathcal{G}_+$ , which together determine how far into  $\mathcal{R}$  the state will diffuse.

Figure 3(a) shows the ratio  $\mathcal{G}_-/\mathcal{G}_+$  as a function of nuclear polarization, averaged over the nuclear initial state distribution,  $p(M)$ . This distribution is taken as thermal at the polarization-dependent temperature  $T$ ,



i.e.,  $p(M) \sim \prod_j \exp[-m_j \omega_Z^n / (k_B T)]$ , where  $k_B$  is the Boltzmann constant [25], for  $I = 3/2$  and  $N \simeq 5 \times 10^4$  [see Fig. 3(a)]. The relative ensemble standard deviations (not shown) are negligible,  $\sim 10^{-3}$ . An important conclusion drawn from Fig. 3(a) is that the  $\zeta = 2$  mode is more robust towards imperfect polarization, owing to the different dependence of the leakage factor  $\mathcal{G}_-/\mathcal{G}_+$  on polarization for  $\zeta = 1$  and  $\zeta = 2$ . The  $\Phi_2^-$  transition becomes dark when the levels  $m = +3/2, m = +1/2$  are depleted, whereas for  $\Phi_1^-$ , the level  $m = -1/2$  needs to be depleted for this to happen. Indeed, the lower levels of a single spin manifold [Fig. 1(b)] will be populated first, as the polarization is decreased, thus enabling the  $\Phi_1^-$  transition before the  $\Phi_2^-$  transition.

Figure 3(b) shows the calculated values of  $\mathcal{G}_+$  as a function of nuclear Zeeman splitting, where the lines indicate a polarization of 50% and the shaded area shows the variation as the polarization is swept from unity (maximum values) to 0 (minimum values). The coupling rate  $\mathcal{G}_+$  is proportional to  $\sin(2\theta)$  for the  $\zeta = 1$  mode and to  $\sin^2 \theta$  for  $\zeta = 2$ . These angular prefactors have been assumed to be unity to maximize the rates shown in Fig. 3(b), which can be converted to rates for any quadrupolar angle by multiplying them with these prefactors.

*State transfer fidelity.*—The state transfer fidelity is defined as the overlap between the initial electron state and the electron state after a full write-read cycle. We initialize the system in the state  $|\psi(0)\rangle = |\phi\rangle \otimes |M\rangle$  and let

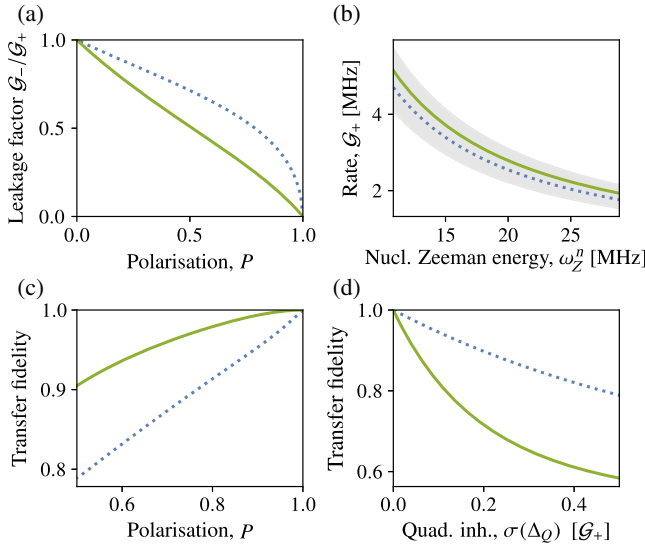


FIG. 3. (a) Leakage factor as ratio of coupling rates,  $\mathcal{G}_-/\mathcal{G}_+$  as a function of nuclear polarization. Green solid (blue dotted) lines denote  $\zeta = 2$  ( $\zeta = 1$ ). (b) Coupling rate  $\mathcal{G}_+$  for  $\zeta = 1$  (blue dotted) and  $\zeta = 2$  (green solid) at  $P = 0.5$  for varying nuclear Zeeman splitting. The shaded area corresponds to the range of values from  $P = 0$  to  $P = 1$ . (c) Transfer fidelity of total write-in and readout cycle as a function of polarization. (d) Transfer fidelity of total write-in and readout cycle at full polarization ( $P = 1$ ) as a function of inhomogeneity in quadrupolar energy shift.

it evolve under the pulse sequence for a time  $t_1$  to write the electron state into the nuclei, thus generating the state  $|\psi(t_1)\rangle$ . After this, we trace out the electron to obtain the reduced nuclear state  $\rho_n(t_1) = \text{Tr}_e[|\psi(t_1)\rangle\langle\psi(t_1)|]$ . To read the nuclear state back into the electron spin, we reinitialize the density operator in the state  $\rho(t_1; 0) = |\downarrow\rangle\langle\downarrow| \otimes \rho_n(t_1)$  and let the system evolve under the pulse sequence for a time  $t_2$ , where the total density operator is  $\rho(t_1; t_2)$ . We then evaluate the overlap of the electron spin state (tracing out the nuclei) with respect to the input state to assess the fidelity  $\mathcal{F}(t_1, t_2) = \text{Tr}_n[\langle\phi'|\rho(t_1; t_2)|\phi'\rangle]$ , where  $|\phi'\rangle = \alpha|\uparrow\rangle - \beta|\downarrow\rangle$ . The fidelity is then averaged over the six states  $(\alpha, \beta) = (1, 0), (0, 1), (1/\sqrt{2})(1, \pm 1), (1/\sqrt{2})(1, \pm i)$ , and there is a unique combination of write-in ( $t_1$ ) and readout ( $t_2$ ) times, found numerically, that maximize this fidelity. In the fully polarized case, the optimal  $t_1$  and  $t_2$  are simply  $\pi/(2\mathcal{G}_+)$ , but as the polarization is decreased, coupling to  $\mathcal{R}$  necessitates slightly ( $< 20\%$ ) longer transfer times. The time-optimized fidelity is presented in Fig. 3(c), which confirms that it follows the polarization dependence of the leakage factor,  $\mathcal{G}_-/\mathcal{G}_+$ , and accordingly that the fidelity is generally higher for the  $\zeta = 2$  mode if the polarization is finite. In particular, for  $\zeta = 2$ , the fidelity remains above 90% throughout the polarization range 50%–100%.

*Adjusting to quadrupolar energy shifts.*—The  $I_z^j$ -commuting contribution to the quadrupolar Hamiltonian can be written as  $H_Q^0 = \sum_j \Delta_Q (I_z^j)^2$ , with  $\Delta_Q = B_Q(\cos^2 \theta - \frac{1}{2}\sin^2 \theta)$ . In general,  $\Delta_Q$  varies over the ensemble, and the individual spin components in the spin wave  $|1\rangle$  evolve with a phase factor  $e^{-i\zeta^2 \Delta_Q^j t}$ , building up a relative phase among the components on a timescale set by the ensemble variation of  $\Delta_Q^j$ , denoted by  $\sigma(\Delta_Q)$ . As a result,  $|1\rangle$  rotates into a dark subspace,  $\{|1_p\rangle\}$ , such that  $\Phi_-|1_p\rangle = 0$  with a rate of  $\gamma = \zeta^2 \sigma(\Delta_Q)$  [25]. In Fig. 3(d), we show how the transfer fidelity at full nuclear polarization depends on this inhomogeneity. As indicated, the energy scale of the inhomogeneity  $\sigma(\Delta_Q)$  must be compared to the coupling rate  $\mathcal{G}_+$  to assess its impact. Thus, with a realistic value of  $\mathcal{G}_+$  in the MHz range, a quadrupolar inhomogeneity below  $\sim 100$  kHz, achievable, e.g., through lattice-matched epitaxial quantum dot growth [33], does not degrade the transfer fidelity appreciably. Importantly, decoherence due to rotation into the dark subspace is only of concern during the transfer process: after the state has been transferred, the collective phase of the nuclear excitation can be refocused through an NMR pulse sequence operating on the  $\{m = -I, m = -I + \zeta\}$  subspace [17,25,34]. In the case of a nonzero mean value of  $\Delta_Q$ , the  $m = -I$  to  $m = -I + \zeta$  transition is shifted by  $\delta = (\zeta^2 - 2I\zeta)\Delta_Q$ . The memory transfer is then simply effectuated by setting the pulse time delay to  $\tau = \ell\pi/(\zeta\omega_Z^n + \delta)$ .

During storage, we expect the dominant nuclear dephasing mechanism that determines the coherence time of the

memory to be the electron-mediated nuclear dipole-dipole interaction, which scales inversely with the electron Zeeman splitting [18]. In the presence of this dephasing mechanism, the coherence time of the nuclear memory is tens of microseconds. If, however, the electron is removed from the quantum dot after its state is transferred to the nuclei, the only dephasing mechanism is the intrinsic neighbor dipole-dipole interaction, and the coherence time can be well into the millisecond regime [16,17,24]. Importantly, the nuclei should be polarized as to increase the electron Zeeman splitting. This way, nuclear polarization leads not only to increased fidelity in the transfer process, but also to a prolonged storage time.

*Conclusion.*—We have proposed a scheme for collective quantum memory, which can reach transfer fidelities for a full read-write cycle as high as 90% with a modest nuclear polarization of 50% for realistic experimental parameters. In addition, the theoretical and experimental techniques we have presented open new possibilities for further exploration and manipulation of the collective nuclear degrees of freedom, for example, the generation of nuclear cat states, squeezed states, and condensates.

We thank E. Chekhovich for helpful discussions. This work was supported by the ERC PHOENICS grant (617985), the EPSRC Quantum Technology Hub NQIT (EP/M013243/1), and the Royal Society (RGF/EA/181068). D. A. G. acknowledges support from St. John's College Title A Fellowship. E. V. D. and J. M. acknowledge funding from the Danish Council for Independent Research (Grant No. DFF-4181-00416). C. L. G. acknowledges support from a Royal Society Dorothy Hodgkin Fellowship.

\* cl538@cam.ac.uk

- [1] H.-J. Briegel, W. Dür, J. I. Cirac, and P. Zoller, *Phys. Rev. Lett.* **81**, 5932 (1998).
- [2] H. J. Kimble, *Nature (London)* **453**, 1023 (2008).
- [3] A. E. Kozhekin, K. Mølmer, and E. Polzik, *Phys. Rev. A* **62**, 033809 (2000).
- [4] B. Julsgaard, J. Sherson, J. I. Cirac, J. Fiurášek, and E. S. Polzik, *Nature (London)* **432**, 482 (2004).
- [5] K. S. Choi, A. Goban, S. B. Papp, S. J. Van Enk, and H. J. Kimble, *Nature (London)* **468**, 412 (2010).
- [6] R. Zhao, Y. O. Dudin, S. D. Jenkins, C. J. Campbell, D. N. Matsukevich, T. A. B. Kennedy, and A. Kuzmich, *Nat. Phys.* **5**, 100 (2009).
- [7] M. P. Hedges, J. J. Longdell, Y. Li, and M. J. Sellars, *Nature (London)* **465**, 1052 (2010).
- [8] W. Tittel, M. Afzelius, T. Chaneliere, R. L. Cone, S. Kröll, S. A. Moiseev, and M. Sellars, *Laser Photonics Rev.* **4**, 244 (2010).
- [9] D. Kielpinski, V. Meyer, M. A. Rowe, C. A. Sackett, W. M. Itano, C. Monroe, and D. J. Wineland, *Science* **291**, 1013 (2001).
- [10] C. Langer, R. Ozeri, J. D. Jost, J. Chiaverini, B. DeMarco, A. Ben-Kish, R. B. Blakestad, J. Britton, D. B. Hume, W. M. Itano *et al.*, *Phys. Rev. Lett.* **95**, 060502 (2005).
- [11] M. V. G. Dutt, L. Childress, L. Jiang, E. Togan, J. Maze, F. Jelezko, A. Zibrov, P. R. Hemmer, and M. D. Lukin, *Science* **316**, 1312 (2007).
- [12] G. D. Fuchs, G. Burkard, P. V. Klimov, and D. D. Awschalom, *Nat. Phys.* **7**, 789 (2011).
- [13] T. H. Taminiau, J. Cramer, T. van der Sar, V. V. Dobrovitski, and R. Hanson, *Nat. Nanotechnol.* **9**, 171 (2014).
- [14] J. M. Taylor, C. M. Marcus, and M. D. Lukin, *Phys. Rev. Lett.* **90**, 206803 (2003).
- [15] J. M. Taylor, A. Imamoglu, and M. D. Lukin, *Phys. Rev. Lett.* **91**, 246802 (2003).
- [16] Z. Kurucz, M. W. Sørensen, J. M. Taylor, M. D. Lukin, and M. Fleischhauer, *Phys. Rev. Lett.* **103**, 010502 (2009).
- [17] E. A. Chekhovich, M. Hopkinson, M. S. Skolnick, and A. I. Tartakovskii, *Nat. Commun.* **6**, 6348 (2015).
- [18] G. Wüst, M. Munsch, F. Maier, A. V. Kuhlmann, A. Ludwig, A. D. Wieck, D. Loss, M. Poggio, and R. J. Warburton, *Nat. Nanotechnol.* **11**, 885 (2016).
- [19] D. A. Gangloff, G. Ethier-Majcher, C. Lang, E. V. Denning, J. H. Bodey, D. Jackson, E. Clarke, M. Hugues, C. Le Gall, and M. Atatüre, *Science* **364**, 62 (2019).
- [20] A. Högele, M. Kroner, C. Latta, M. Claassen, I. Carusotto, C. Bulutay, and A. Imamoglu, *Phys. Rev. Lett.* **108**, 197403 (2012).
- [21] I. Schwartz, J. Scheuer, B. Tratzmiller, S. Müller, Q. Chen, I. Dhand, Z.-Y. Wang, C. Müller, B. Naydenov, F. Jelezko *et al.*, *Sci. Adv.* **4**, eaat8978 (2018).
- [22] J. H. Bodey, R. Stockill, E. V. Denning, D. A. Gangloff, G. Ethier-Majcher, D. M. Jackson, E. Clarke, M. Hugues, C. Le Gall, and M. Atatüre, [arXiv:1906.00427](https://arxiv.org/abs/1906.00427).
- [23] W. Yao, R.-B. Liu, and L. J. Sham, *Phys. Rev. B* **74**, 195301 (2006).
- [24] C. Deng and X. Hu, *IEEE Trans. Nanotechnol.* **4**, 35 (2005).
- [25] See Supplemental Material at <http://link.aps.org/supplemental/10.1103/PhysRevLett.123.140502> for detailed derivations and descriptions of the results, which includes Refs. [26–29].
- [26] B. Urbaszek, X. Marie, T. Amand, O. Krebs, P. Voisin, P. Malentinsky, A. Högele, and A. Imamoglu, *Rev. Mod. Phys.* **85**, 79 (2013).
- [27] Y. H. Huo, B. J. Witek, S. Kumar, J. R. Cardenas, J. X. Zhang, N. Akopian, R. Singh, E. Zallo, R. Grifone, D. Kriegner *et al.*, *Nat. Phys.* **10**, 46 (2014).
- [28] J. R. Johansson, P. D. Nation, and F. Nori, *Comput. Phys. Commun.* **184**, 1234 (2013).
- [29] E. A. Chekhovich, I. M. Griffiths, M. S. Skolnick, H. Huang, S. F. Covre da Silva, X. Yuan, and A. Rastelli, *Phys. Rev. B* **97**, 235311 (2018).
- [30] C. Bulutay, *Phys. Rev. B* **85**, 115313 (2012).
- [31] X. Yuan, F. Weyhausen-Brinkmann, J. Martín-Sánchez, G. Piredda, V. Krápek, Y. Huo, H. Huang, C. Schimpf, O. G. Schmidt, J. Edlinger *et al.*, *Nat. Commun.* **9**, 3058 (2018).
- [32] K. Flisinski, I. Y. Gerlovin, I. V. Ignatiev, M. Y. Petrov, S. Y. Verbin, D. R. Yakovlev, D. Reuter, A. D. Wieck, and M. Bayer, *Phys. Rev. B* **82**, 081308(R) (2010).
- [33] E. A. Chekhovich, A. Ulhaq, E. Zallo, F. Ding, O. G. Schmidt, and M. S. Skolnick, *Nat. Mater.* **16**, 982 (2017).
- [34] B. Albrecht, P. Farrera, G. Heinze, M. Cristiani, and H. de Riedmatten, *Phys. Rev. Lett.* **115**, 160501 (2015).